ACS OMEGA

Open Access

http://pubs.acs.org/journal/acsodf

Article

Composite Flame Retardants Based on Conjugated Microporous Polymer Hollow Nanospheres with Excellent Flame Retardancy

Chonghua Ma,* Min Su, and Zhaoqi Zhu*

Cite This: *ACS Omega* 2024, 9, 10478−10487

Read Online

ACCESS | Metrics & More | Article Recommendations

ABSTRACT: The development of polymer materials with excellent flame retardancy has been paid increasing attention for their valuable applications in saving energy in modern architecture. Herein, conjugated microporous polymers hollow nanospheres (CMPs-HNS) were prepared by Sonogashira−Hagihara cross-coupling reaction with 1,3,5-triacetylenebenzene, 3-amino-2,6-dibromopyridine, and 2,4,6-tribromoaniline as building blocks using SiO_2 nanoparticles as hard templates. To enhance the flame-retardant performance of the CMPs-HNS, antimony pentoxide solution (Sb_2O_5) and bisphenol A-bis (diphenyl phosphate) (BDP) were coated onto the as-prepared CMP-HNS (CMPs-HNS-BSb) by a simple immersion method. The peak heat release (pHRR) from microscale combustion colorimeter (MCC) of CMPs-HNS-BSb was 76.5 and 73.05 W g^{-1}, respectively. By introducing CMPs-HNS-BSb into the epoxy resin (EP) matrix, the CMP2-HNS-BSb/EP (0.5) composites show that the pHRR values were 809.3 and 645.2 kW m^{-2}, reduced by 21% as measured by conical calorimetry (CC), and total heat release (THR) reduced by 29.7%, going from 101 to 70.8 MJ/m^2 when compared to the pure sample. Besides, total smoke production (TSP) reduced about 23.7%. The hollow structure can enhance the thermal insulation performance. As measured, the thermal conductivity of CMP1-HNS-BSb and CMP2-HNS-BSb is 0.044 and 0.048 W m^{-1} K^{-1}. Based on the advantages of simple manufacture, superior thermal insulation, and flame retardancy, our CMPs-HNS-BSb/EP composites may find useful applications in various aspects such as building energy saving in future development.

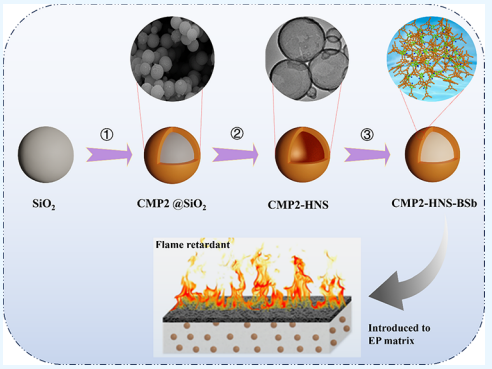

1. INTRODUCTION

In recent years, fire accidents caused by exterior wall thermal insulation materials in the construction industry have continually happened[1,2] and fires usually cause casualties. The development of an excellent flame-retardant material has attracted extensive attention for its valuable applications in saving energy in architecture. However, a large number of building materials such as polyvinyl chloride,[3] polypropylene,[4] polystyrene,[5] styrene butadiene rubber,[6] and fiber[7] belong to flammable materials. Once a fire occurs, the combustion of these polymers will cause serious fire accidents, resulting in casualties and property losses. According to literature research, an average of 10 people were dead in fires every day in the United States.[8] Therefore, the research and preparation of flame-retardant materials is still a research hotspot in the modern construction industry.

To date, most flame-retardant materials can be divided into organic materials, inorganic materials, and composite materials with their physical and chemical structure properties. Inorganic flame-retardant materials are generally made up of nonrenewable energy sources, including mineral wool, foam glass,[9] and so on, and they are generally low cost, have good ecological and environmental protection, and are easy to recycle and reuse.[8,10,11] Organic flame retardant materials[12−15] include epoxy resin, polyurethane foam,[16−18] polystyrene board,[19] phenolic foam,[20,21] cellulose,[22,23] rubber,[24,25] etc. Although organic flame-retardant materials have the advantages of high specific surface area, good adsorption performance, and good thermal stability,[26,27] some problems, such as poor nonaging resistance,[28] large deformation coefficient,[29] and easy combustion[30] limited their usage in many areas. To make the materials with both flame retardant and thermal insulation, nanoadditives such as graphene sheets[31] and carbon sheets[32] can be introduced.[33] For example, Liu et al.[34] synthesized dimelamine pyrophosphate from melamine and sodium pyrophosphate and introduced it to EP. During combustion, the dense carbon layer that can be developed during the combustion process, along with the nonflammable gases released, significantly enhances the flame-retardant capability. Qiao et al.[35] introduced hollow

Received: October 30, 2023
Revised: January 28, 2024
Accepted: February 2, 2024
Published: February 22, 2024

glass microspheres into EP via a combination of templates and a simple casting method. Compared with pure EP, the density was reduced by 39.16%, and thermal conductivity was reduced by 37.31%.

Conjugated microporous polymers[36] (CMPs), as a kind of advanced porous organic polymers (POPs), have attracted much more attention due to good thermal stability,[37] high physical and chemical stability,[38,39] high specific surface area,[40] and their potential application in various aspects such as separation,[41] catalysis,[42] storage, adsorption, and energy storage and conversion.[43] Recently, our group has reported many works on CMPs in the field of thermal insulation and flame retardancy. Wei[44,45] has reported for the first time that benzotriazole-conjugated microporous polymers (ZCMPs) with flame retardant properties were obtained by Sonogashira-Hagihara cross-coupling polymerization in 2017. Wu[46] designed and prepared two kinds of CMP nanotube-based composites (M-CMPN1 and M-CMPN2). However, only with the addition of magnesium hydroxid in M-CMPN with high load levels, do the additives display a better flame retardancy. Thus, further exploitation of high-performance CMPs-based flame retardants with high flame retardancy to meet practical industrial applications is of great interest.

In this work, we reported the synthesis of CMPs hollow nanosphere (CMPs-HNS) based flame retardant materials using a simple immersion method. The CMPs-HNS shows high specific surface area (327.6 and 483.5 $m^2\ g^{-1}$, respectively) and superhydrophobicity (164.2° and 166.8°), while CMPs-HNS-BSb shows high thermal stability (thermal decomposition temperature was 285 and 320 °C, respectively). The peak heat release (pHRR) from microscale combustion colorimeter (MCC) of CMPs-HNS-BSb was 76.5 and 73.05 W g^{-1}, respectively. The pHRR value from conical calorimetry (CC) of CMP2-HNS-BSb/EP reached 645.03 kW m^{-2} when only 0.5 g of CMP2-HNS-BSb was added to EP. Compared with pure EP, the composite with flame retardant has a remarkable flame-retardant effect. We highlighted that the water, phosphoric acid, and PO· free radicals produced after CMPs-HNS-BSb combustion would dilute oxygen and inhibit the combustion of polymers. Thus, CMPs have the potential for practical application as a new flame-retardant material. Our research also provides new possibilities for the development of composite materials with good flame-retardant properties in the future and is expected to be applied in a variety of fields such as aerospace and architecture.

2. MATERIALS AND METHODS

2.1. Materials. 1,3,5-Triacetylenebenzene was received from TCI (Shanghai, China). 2,4,6-Tribromoaniline, cuprous iodide (CuI), and tetrakis(triphenylphosphine)palladium(0) Pd(0) were all supplied from BlackWell Technology Co., Ltd. 3-Amino-2, 6-dibromopyridine and bisphenol A-bis(diphenyl phosphate) (BDP) were all obtained from J&K Chemical Co., Ltd. Silica nanoparticles (approximately 200 nm) were applied from Shanghai Buwei Applied Materials Technology Co., Ltd. Phoenix epoxy resin (EP) was purchased from Nantong Xingchen Synthetic Material Co., Ltd. Low molecular weight polyamide resin (PA-650) was purchased from Shandong Deyuan Epoxy Technology Co., Ltd. Hydrofluoric acid (HF) was supplied from Shanghai Aladdin Biochemical Technology Co., Ltd. Antimony pentoxide (Sb_2O_5) was obtained by self-made using sodium antimonate received from Macklin Biochemical Co., Ltd. (Shanghai). Toluene, triethylamine, acetone, chloroform, methyl alcohol, and other solvents were obtained from Tianjin Fuyu Chemical Reagent Co., Ltd. The above solvents were all analytical grade; thus, purification was not essential.

2.2. Methods. *2.2.1. Synthesis of SiO_2@CMPs.* First, CuI (4 mg, 0.021 mmol), Tetrakis(triphenylphosphine) palladium(0) (46 mg, 0.066 mmol), silica nanospheres (783 mg), toluene (30 mL), and triethylamine (30 mL) were added to a 100 mL custom-made flat bottom glass tube. After ultrasonic treatment, 1,3,5-triacetylbenzene (60 mg, 0.4 mmol) and 3-amino-2,6-dibromopyridine were added to the tube (151 mg, 0.6 mmol), and nitrogen was injected into the mixture for 20 min to ensure that the reactants are not oxidized. The mixture was reacted continuously at 90 °C for 48 h. After the reaction, the mixed product was cooled to room temperature, washed with chloroform, acetone, and methanol several times, extracted with methanol Soxhlet for 72 h, and dried at 70 °C until the mass was constant; it was named SiO_2@CMP1.

2.2.2. Synthesis of SiO_2@CMP2. CuI (2 mg,0. 011 mmol) and Pd (0) (23 mg, 0.02 mmol) were used to catalyze the cross-coupling reaction of 1,3,5-triacetylenebenzene (30 mg, 0.2 mmol) and 2,4,6-tribromoaniline (66 mg, 0.3 mmol), the reaction temperature was 80 °C, and the other steps were the same compared with SiO_2@CMP1.

2.2.3. Synthesis of the Sb2O5 Hydrogel. The Sb_2O_5 hydrogel was prepared by the sodium antimonate gel sol method. First, water was added to sodium antimonate, stirred, and dispersed, and the concentration was 0.3 g/mL. Then, 35% hydrochloric acid was added under stirring and heated to 40 °C, and the mixture was reacted for 4 h. antimony pentoxide gel slurry was obtained.After filtration and separation and washing with pure water, the antimony pentoxide filter cake obtained was added to pure water and then to triethanolamine and heated to 75 °C for desolvation for 5 h to produce antimony pentoxide sol product. After filtration and separation and washing with pure water, the antimony pentoxide filter cake obtained was added to pure water and then to triethanolamine and heated to 75 °C for peptizing for 5 h to produce antimony pentoxide sol product.

2.2.4. Synthesis of CMPs-HNS and CMPs-HNS-BSb. The SiO_2@CMPs (0.35 g) obtained above were added to a 50 mL plastic beaker, mixed with water (15 mL), methanol (20 mL), and HF (7.5 mL), and soaked at room temperature for 4 h. The mixed system was washed several times with acetone, water, and methanol, dried to constant weight at 70 °C, and named CMP1-HNS and CMP2-HNS, respectively. The as-prepared above CMPs-HNS were placed in a Petri dish, and the Sb_2O_5 hydrogel prepared was added to soak, then, BDP solution was added by similar methods for 4 h, and finally the excess BDP solution and Sb_2O_5 solution was filtered out to obtain CMP1-HNS-BDP/Sb_2O_5 (C1-H-BSb) and CMP2-HNS-BDP/Sb_2O_5 (C2-H-BSb).

2.2.5. Synthesis of EP and EP complexes. Formula is as follows (Table 1).

2.3. Characterization. The ^{13}C cross-polarization magic angle spinning (CP/MAS) nuclear magnetic resonance (NMR) spectra and Fourier transform infrared (FTIR) spectra were used to characterize the structure of the CMPs-HNS. The micromorphology of the sample was observed by a JSM-6701F cold-field emission scanning electron microscope (SEM) produced by Japan Electronics Corporation (JEOL). The INCA EDS tester of Oxford

https://doi.org/10.1021/acsomega.3c08597
ACS Omega 2024, 9, 10478−10487

Table 1. EP and EP Composite Material Composition Addition Table

samples	EP, g	PA-650, g	C1-H-BSb, g	C2-H-BSb, g
pure/EP	48	32	0	0
C1-H-BSb(0.5)/EP	48	32	0.5	0
C1-H-BSb(1.5)/EP	48	32	1.5	0
C2-H-BSb(0.2)/EP	48	32	0	0.2
C2-H-BSb(0.5)/EP	48	32	0	0.5

Instrument Company was used to observe the distribution and compositions of relative elements of CMPs@. Transmission electron microscopy (TEM) produced by FIE Company in the United States was used to test and observe the shape, size, and other details of the samples. The thermal stability of the samples CMPs-HNS-BSb was analyzed by thermogravimetric analyzer TGA (Pyris1) produced by PerkinElmer Company in the United States. The porosity of the samples was obtained by the Brunauer−Emmett−Teller (BET) carried out by the ASAP 2020 instrument produced by Micromeritics, USA. The contact angle of water (CA) of CMPs-HNS was measured by using a CA meter (DSA100, Kruss), and the data were analyzed. The microcalorimetry (MCC) test was performed using the miniature combustion calorimeter manufactured by GOV-MARK Company. The test conditions were as follows: the heating rate was 1 °C/s and the temperature range was from room temperature to 800 °C. Conical calorimetry (CC) tests were performed on a VOUCH-6810 system in accordance with ISO5560 standards. Each specimen (100 × 100 × 3 mm^3) was coated with aluminum foil, and the data were scanned every 5 s at a test voltage of 35 kV.

3. RESULTS AND DISCUSSION

Figure 1a shows the synthesis diagram of CMPs-HNS-BSb. In this study, silica nanospheres were used as templates, and 1,3,5-trisynylbenzene, 3-amino-2, 6-dibromopyridine, and 2,4,6-tribromoaniline were synthesized as monomers to obtain CMPs@SiO_2. After that, SiO_2 was etched by HF to obtain CMPs-HNS. Finally, the flame retardants CMP-HNS-BSb were obtained by soaking them with BDP and Sb_2O_5. As shown in Figure 1a, b, it is the synthesis reaction equation of CMP1-HNS and CMP2-HNS, respectively. This kind of reaction is the Sonogashira-Hagihara cross-coupling reaction, that is, the reaction between halogenated monomer and terminal alkyne in toluene and triethylamine as solvent.[47] Figure 1c, d is the molecular simulation of CMP1-HNS and CMP2-HNS, respectively, which shows that the microstructure is a three-dimensional network and has good stability.

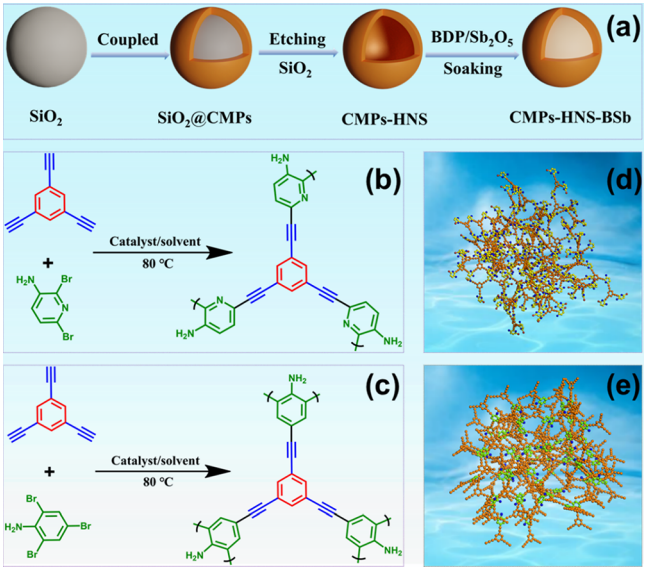

Figure 1. (a) Synthesis route of CMPs-HNS, (b, c) synthesis method of CMP1-HNS and CMP2-HNS, and (d, e) molecular simulation of CMP1-HNS and CMP2-HNS.

The morphology of samples CMPs@SiO_2 and CMPs-HNS-BSb was observed by SEM and TEM. As can be seen from Figure 2a, b, the microstructure of CMP1@SiO_2 is spherical because it is supported by SiO_2 nanospheres, and CMP1 reacts on the nanospheres, thus forming a "shell".[48] In addition, the spheroids are uniform in size with an average particle size of about 250 nm. The CMP1@SiO_2 sphere etched by HF has an obvious hollow structure, as can be seen in Figure 2c, which is consistent with our expectation. Figure 2d shows the element distribution of CMP1@SiO_2, where O elements are derived from SiO_2, and C and N elements are derived from synthesized CMP1. As can be seen from the element distribution diagram, the N element is significantly less than C and O because there is less N element in the halogenated monomer.[49] As shown in Figure 2e, f, the morphology of CMP2@SiO_2 and CMP1@SiO_2 is very similar and is uniformly spherical. After etching CMP2@SiO_2 with a mixture of methanol, water, and HF,[50] the completely hollow sphere CMP2-HNS was obtained. TEM data from Figure 2g showed that CMP2-HNS completely maintained the shape of the sphere and no defects such as collapse were found, which indicated that CMPs had good stability. Similarly, Figure 2h shows the element distribution of CMP2@SiO_2, and its element content trend is similar to CMP1@SiO_2. As shown in Figure 3a−d, CMP1-HNS-BSb maintains the hollow sphere structure, which is helpful for thermal insulation. In the TEM and SEM images from Figure 3e−h, the presence of a coating on the sphere surface is clearly observable, providing conclusive evidence of the successful coating of BDP and Sb2O5. Figure 2i, j shows the distribution of elements of CMP1-HNS-BSb and CMP2-HNS-BSb, respectively. Unlike CMP1@SiO_2 and CMP2@SiO_2, they contain P elements and Sb elements because CMPs-HNS were soaked in BDP and Sb_2O_5.

To determine the structure of CMPs-HNS, FTIR and NMR spectroscopy were used to characterize them. As shown in Figure 4a, the hole peak of 3500−3000 cm^{-1} in the FTIR spectrum is the characteristic peak of $-NH_2$,[49] and the appearance of this peak indicates that the halogenated monomer is successfully bonded to 1,3,5-trisynylbenzene. In addition, the characteristic peak at 2980 cm^{-1} is the stretching vibration of substituted benzene aromatic hydrocarbon $C_{Ar}-H$. The peak at 2290−2200 cm^{-1} is the stretching vibration peak of $-C\equiv C-$, where the peak is basically not obvious, which is attributed to the symmetric structure of CMPs-HNS.[51] The multiple peaks at 1610 and ∼1000 cm^{-1} belong to the vibration peak of the conjugate system on the aromatic ring. The FTIR spectrum of CMP2-HNS is similar to CMP1-HNS in that they contain similar functional groups.

https://doi.org/10.1021/acsomega.3c08597
ACS Omega 2024, 9, 10478−10487

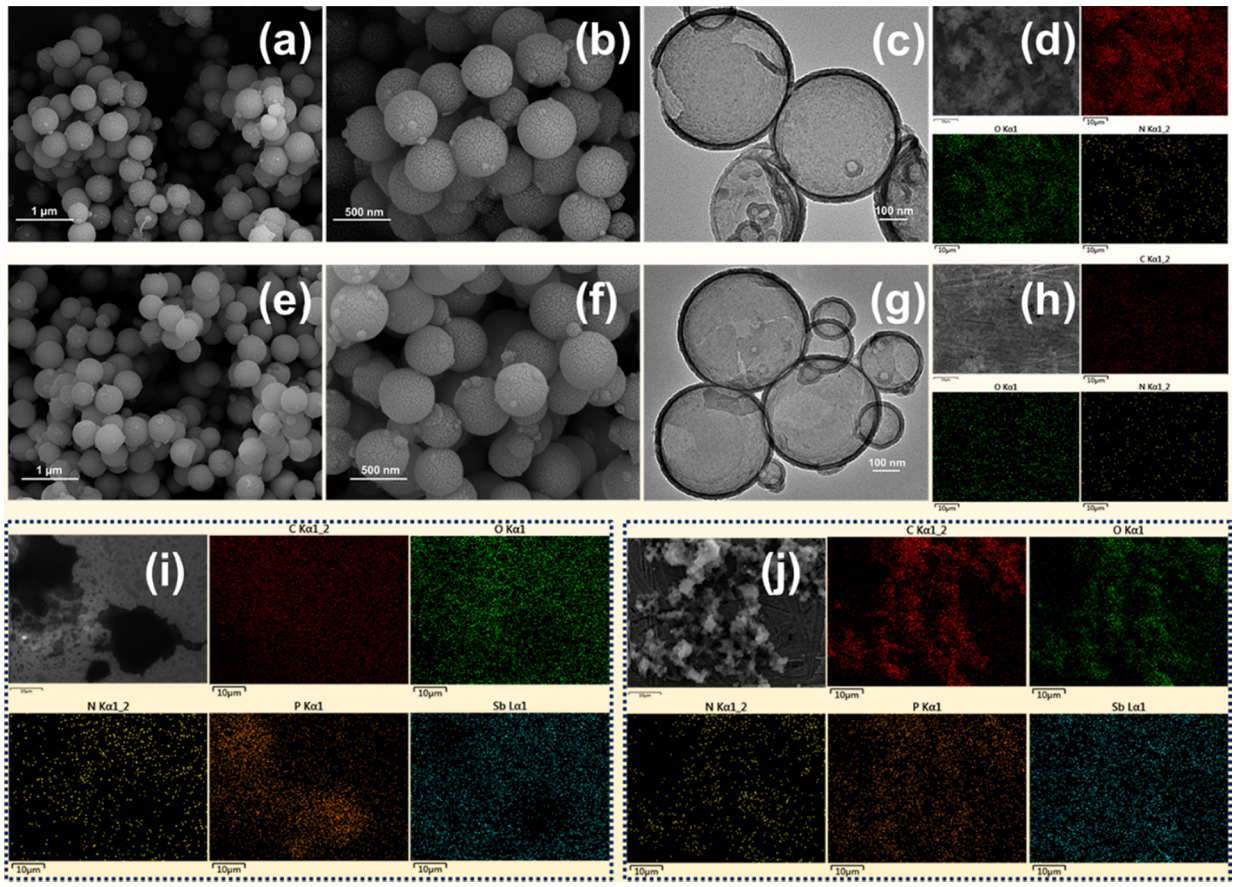

Figure 2. (a and b) SEM images of CMP1@SiO_2. (c) TEM images of CMP1-HNS. (d) EDS images of CMP1@SiO_2. (e and f) SEM images of CMP2@SiO_2. (g) TEM images of CMP1-HNS. (h) EDS images of CMP2@SiO_2. (i) EDS images of CMP1-HNS-BSb. (j) EDS images of CMP2-HNS-BSb.

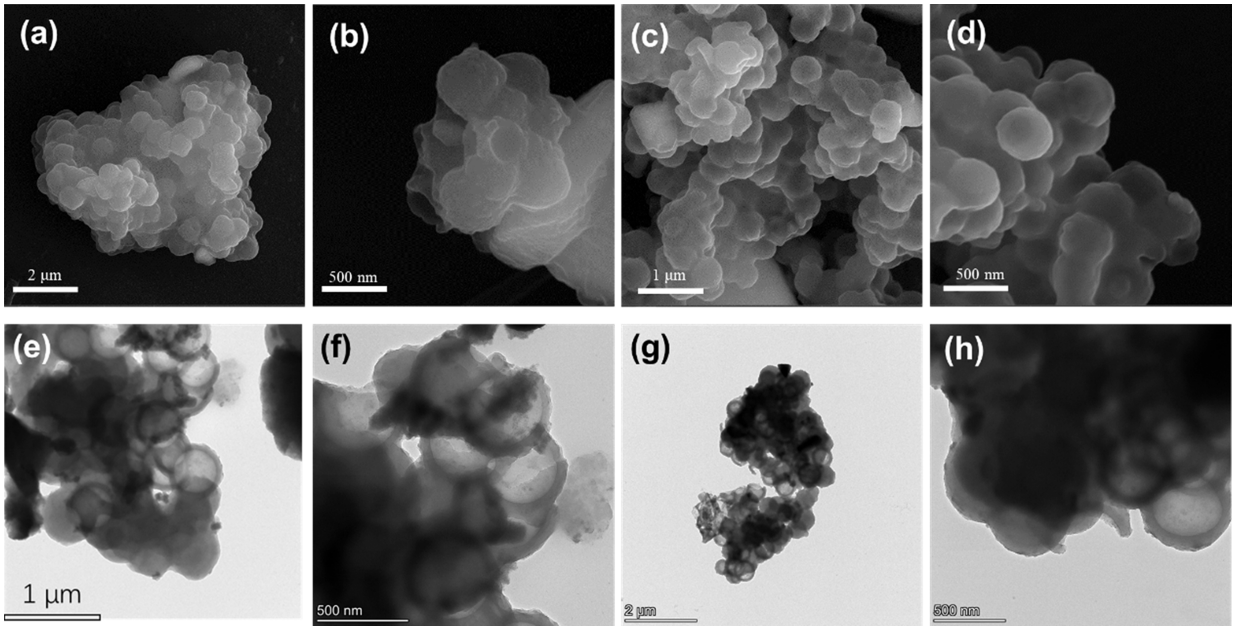

Figure 3. (a and b) SEM images of CMP1-HNS-BSb. (c, d) SEM images of CMP2-HNS-BSb. (e, f) TEM images of CMP1-HNS-BSb. (g, h) TEM images of CMP2-HNS-BSb.

Besides, we calculated the loading capacity of BDP and Sb_2O_5. After treatment by BDP and Sb_2O_5, the mass of 0.75 g of CMP1-HNS increased by 0.5793 g from 0.75 to 1.3293 g, which represents a 77.2% increase. CMP2-HNS shows an increase of 63.5% from 0.75 to 1.226 g. The loading amounts of BDP and Sb_2O_5 are notable.

https://doi.org/10.1021/acsomega.3c08597
ACS Omega 2024, 9, 10478−10487

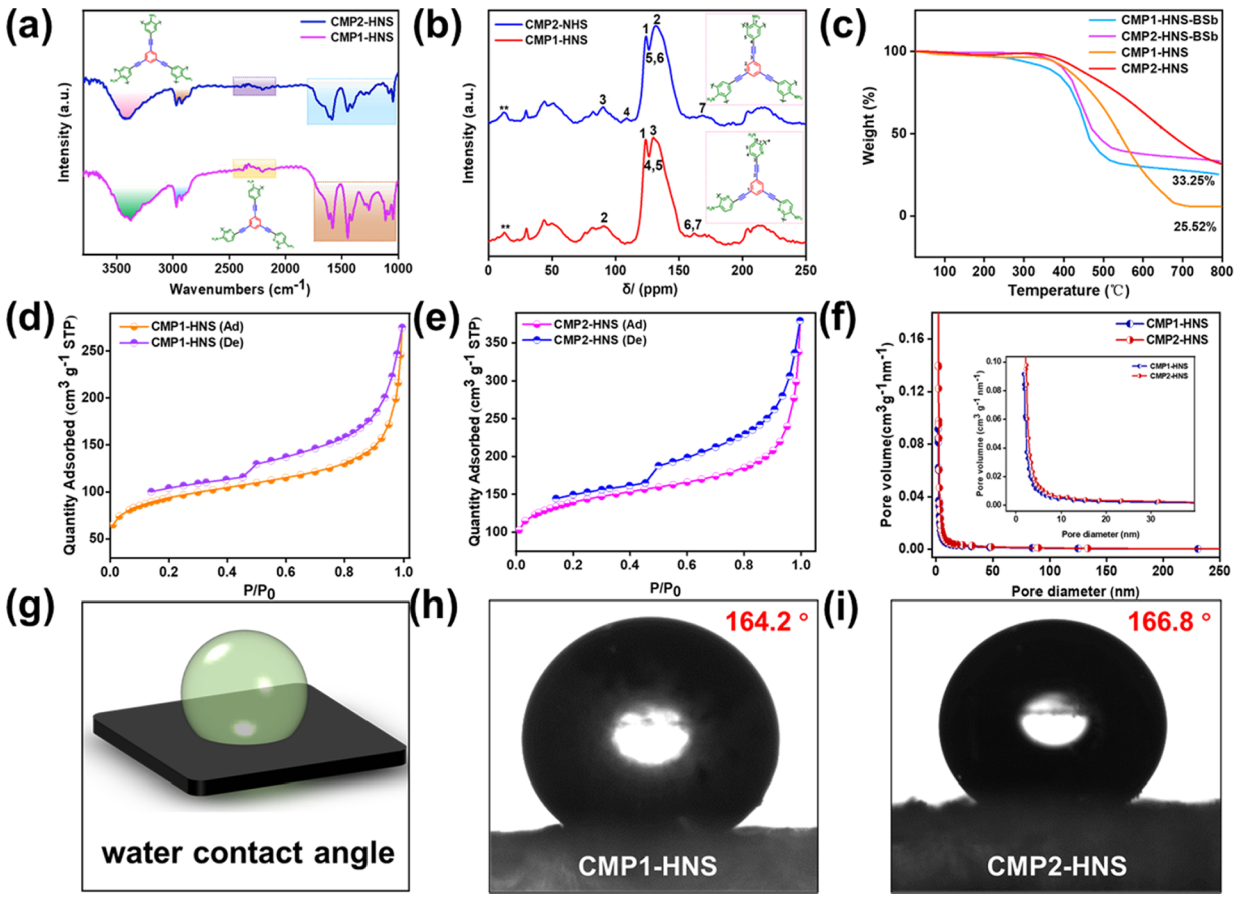

Figure 4. (a) FTIR spectra of CMPs-HNS, (b) ^{13}C CP/MAS NMR spectra of CMPs-HNS, (c) TGA curves of CMPs-HNS and CMPs-HNS-BSb under nitrogen. (d, e) Pore size distribution curves of CMP1-HNS and CMP2-HNS, calculated according to adsorption data. (g) Simulation diagram of water contact angle. (h, i) Water contact angle of CMP1-HNS and CMP2-HNS, respectively.

Table 2. Porous Properties of CMP1-HNS and CMP2-HNS; (Three Repeated Trials) [Micropore and Macropore (mic-mac) and Adsorption Average Pore Width (*D* pore)]

samples	S_{BET} (m^2 g^{-1})	$S_{mic\text{-}mac}$ (m^2 g^{-1})	$V_{mic\text{-}mac}$ (cm^3 g^{-1})	V_{tot} (cm^3 g^{-1})	D_{pored} (nm)
CMP1-HNS	327.6	195.4	0.38	0.38	4.64
CMP2-HNS	483.5	413.9	0.52	0.58	4.33

In order to further observe the structural characteristics of CMPs-HNS, NMR spectroscopy was used to analyze the structures of the two as-synthesized samples. As can be seen in Figure 4b, for CMP1-HNS, the sharp peak at 121.9 ppm is the position of the C element at the benzene ring triple substitution, indicating the presence of the benzene ring. The peak at 135.8 ppm is the unsubstituted position on the benzene ring. The existence of this peak indicates that the halogenated monomer is not reflected there, which is consistent with the synthesis equation. In addition, the peak at δ = 86.9−90.2 ppm shows the position of −C≡C−.[52] The position of δ = 132.4 ppm is the position of alkynyl benzene substitution, and this is the position of the reaction between the terminal alkynyl group and the halogenated monomer, which proves that the reaction is successful. The peak at 142−146 ppm is the amino-substituted C and *ortho*-C position of 3-amino-2,6-dibromo-pyridine.[53] The peak near δ = 16 ppm is attributed to the halogenated element of the halogenated monomer, and this position can continue to react with the terminal alkyne to obtain a larger network structure. The position of the characteristic peak of CMP2-HNS is similar to CMP1-HNS.

The TGA curve is mainly used to detect the thermal stability of CMPs-HNS-BSb and CMPs-HNS under a nitrogen atmosphere. As can be seen from Figure 4c, all the samples can remain basically stable between 0 and 300 °C with little change in sample loss. The thermal decomposition temperature of CMP1-HNS-BSb is about 285 °C, while CMP2-HNS-BSb is about 320 °C, which is higher than 35 °C than CMP1-HNS-BSb, indicating that CMP2-HNS-BSb has good thermal stability. Compared with CMPs-HNS, which have excellent thermal stability, the curves of CMPs-HNS-BSb show that thermal stability has been weakened. It may be due to the loading of BDP. From the whole decomposition process, the curve of CMP1-HNS-BSb is always below that of CMP2-HNS-BSb, which indicates that the thermal stability of CMP2-HNS-BSb is always better than that of CMP1-HNS-BSb from 0 to 800 °C. When the temperature reaches 800 °C, the mass of CMP1-HNS-BSb is only 25.52%, while CMP2-HNS-BSb is 35%, which is 7.73% higher than CMP1-HNS-BSb.

https://doi.org/10.1021/acsomega.3c08597
ACS Omega 2024, 9, 10478−10487

As shown in Figure 4d, e, the porosity of the CMPs-HNS was evaluated by N_2 adsorption−desorption measurements. Both curves belong to the type IV adsorption curve,[54] that is, the desorption curve is above the adsorption curve. The surface areas of CMP1-HNS and CMP2-HNS were determined using N_2 adsorption/desorption isotherms based on the Brunauer−Emmett−Teller (BET) theory which was 327.6 and 483.5 $m^2\ g^{-1}$, respectively. The total pore volumes (V_{tot}) were 0.38 and 0.52 $cm^3\ g^{-1}$, respectively from Table 2. In addition, Figure 4d, e showed that strong nitrogen adsorption in the relative pressure (P/P_0) range of 0.8 to 1.0 indicated the presence of large pores in CMPs-HNS. In addition, the total pore volumes of CMP1-HNS and CMP2-HNS were 0.38 and 0.58 $cm^3\ g^{-1}$, respectively. As shown in Figure 4f, there remained not only micropores but also macropores and mesopores in the composite. As shown in Table 2, according to the pore diameter distribution based on density functional theory (DFT),[49,55] the average pore diameter was about 4.64 and 4.33 nm, respectively.

The water contact angle (CA) was used to analyze the hydrophobic properties of the materials. Figure 4g shows the simulation diagram of the CA on materials. As can be seen from Figure 4g, h, the CA of CMP1-HNS is 164.2°, while the CA of CMP2-HNS is 166.8°. Both of those show superhydrophobicity, which makes the material have good self-cleaning ability and can show low thermal conductivity in humid environments while making the material have an insulation effect. In addition, the two materials are extremely lipophilic.[56] Amounts of studies have shown that when organic solvents such as hexane and acetone touch the sample surface, they will be completely infiltrated in a short time. This property allows the flame retardants BDP and Sb_2O_5 to enter the cavity.[57]

The flame retardancy of CMPs-HNS-BSb was studied by microscale combustion calorimetry (MCC). Figure 5 shows

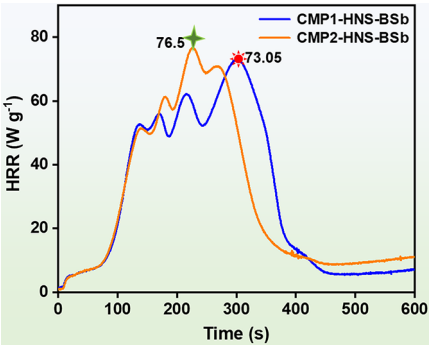

Figure 5. HRR curves of CMP1-HNS-BSb and CMP2-HNS-BSb from MCC.

the relationship between time and the heat release rate (HRR). HRR is the amount of heat released per unit time by the combustion of a material under specified test conditions.[58] The larger the HRR is, the more heat is fed back to the material surface by combustion, which results in a faster pyrolysis speed of the material and increased production of volatile combustible substances, thus accelerating the propagation of flame. The pHRR value of CMP1-HNS-BSb is 73.05 W g^{-1}, while CMP2-HNS-BSB is 76.5 W g^{-1}. Both pHRR values are less than 100 W g^{-1}, which is lower than most reported materials, indicating that the materials have excellent flame-retardant property.[59]

In order to further investigate the flame retardancy of CMPs-HNS-BSb, it was introduced into epoxy resin (EP) as a flame-retardant filler in different proportions. Conical calorimetry[44,60] (CC) is a kind of basis for testing the combustion performance of materials and its principle is the state of oxygen consumed when substances burn. CC test data mainly include heat release rate (HRR), total heat release (THR), total smoke release (TSP), and CO_2P. Among them, from HRR, it could be seen that the higher the HRR is, the easier the material will burn. As shown in Figure 6a and Table 3, the pHRR value of pure EP is the highest, which means that it was the most flammable and the EHC value of the pure sample also is the highest. With the introduction of flame retardants, the pHRR value of EP reduced, indicating that the addition of nanofillers had a flame retarding effect on EP. Among of them, the pHRR of C1-H-BSb (0.5) was 643.80 kW m^{-2}, which was 14.87% lower than pure EP. EHC (effective heat combustion) of C1-H-BSb (0.5)/EP also shows the same trend and is reduced by 18.3%. In addition, the pHRR values of C2-H-BSb were lower than those of C1-H-BSb, which was consistent with the TGA data, indicating that CMP2-HNS-BSb had higher stability and better flame retardant performance, which may be due to the difference in monomer selection and the higher nitrogen content of 2,4,6-tribromoaniline.

Total heat release (THR) refers to the total heat generated when a material is set on fire at a predetermined level of radiation until it goes out. And (effective heat combustion) EHC shows the heat released by a unit of fuel when it is completely burned. Figure 6b, c mainly showed the formation of a carbon layer after CMPs-HNS-BSb combustion, where the layer of carbon provided a strong protective barrier that prevented oxygen and heat from being transferred to the base material, and it could be explained by the large and wide platform peak. According to EHC data shown in Table 3, the CMPs-HNS-BSb helps reduce the EHC of EP obviously, C2-H-BSb (0.5)/EP reduced by 33.38%, which proves the good flame-retardant property of CMPs-HNS-BSb.

Pure EP and CMPs-HNS-BSb/EP samples were prepared by using molds, as shown in Figure 7a. The addition of flame retardant resulted in a slight color change in the samples. They can be molded into various shapes. In order to test the compatibility of CMPs-HNS-BSb with epoxy resin, we tested the toughness of the composites by using a universal testing machine, as shown in Figure 7b, c. In Figure 7b, at lower CMP1-HNS-BSb addition, the toughness of the additive to the matrix of the epoxy resin was reduced. With the increase of the additive amount, the toughness was gradually enhanced. The reason for analyzing this may be due to the better compatibility of nanospheres with an epoxy resin matrix, and the nanoparticles can absorb the crack extension energy well when the matrix is impacted. CMP2-HNS-BSb in the EP matrix also showed a similar trend.

4. MECHANISM OF THE FLAME RETARDANT

During the combustion process, CMP nanospheres have good thermal stability and can be used as a carrier of Sb_2O_5 and BDP, which can also release the incombustible gas as well as its hollow structure during combustion to play the role of blocking the internal heat transfer.[49] BDP in the combustion process, the decomposition at high temperatures to produce

https://doi.org/10.1021/acsomega.3c08597
ACS Omega 2024, 9, 10478−10487

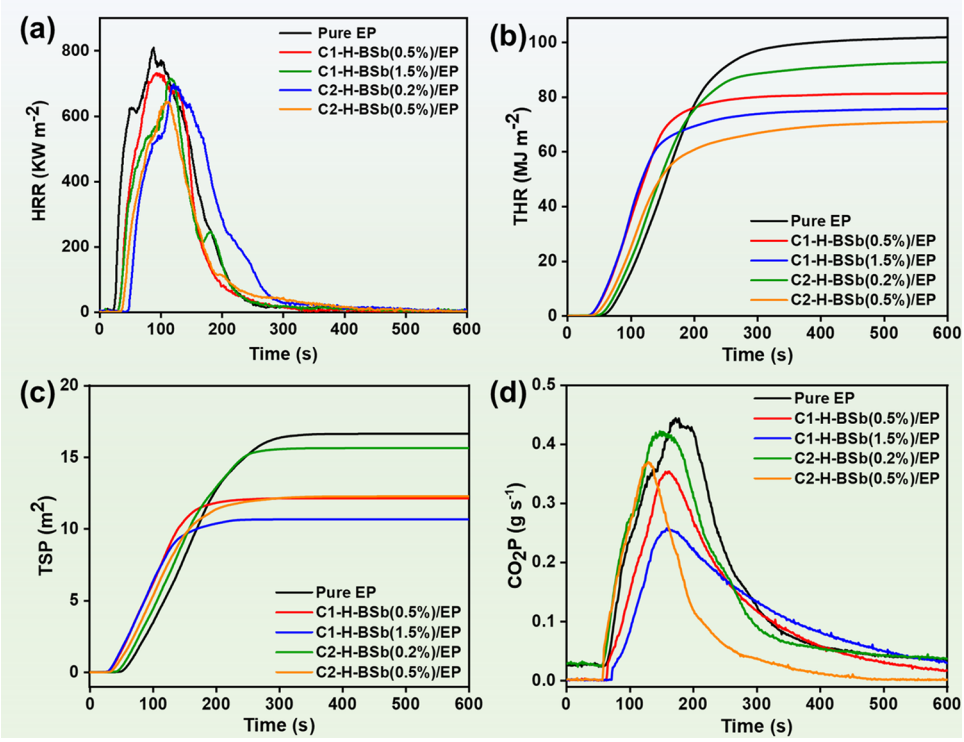

Figure 6. (a) HRR curves of the EP composite materials, (b) THR curves of the EP composite materials, (c) TSP curves of the EP composite materials, and (d) CO_2P curves of the EP composite materials.

Table 3. CC Data of the EP Composite

samples	pHRR (kW m^{-2})	THR (MJ m^{-2})	TSP (m^2)	CO_2P (g s^{-1})	EHC (MJ/kg)
pure EP	756.23	101.82	16.62	0.44	27.74
C1-H-BSb(0.5)/EP	732.09	81.31	12.26	0.35	22.65
C1-H-BSb(1.5)/EP	739.78	75.74	10.66	0.26	23.89
C2-H-BSb(0.2)/EP	698.11	92.96	14.96	0.42	23.43
C2-H-BSb(0.5)/EP	643.80	71.03	12.12	0.37	18.48

phosphorus-containing radicals, such as PO˙, P˙, they can react with the H and OH radicals in the flame to inhibit the propagation of the flame.[61,62] It has been reported that the introduction of antimony flame retardants in the phosphorus flame retardants can also achieve a certain synergistic effect, which can play a good role in suppressing the performance of smoke as well as reduce the use of phosphorus flame retardants.[63]

As shown in Figure 8, the introduction of CMP1-HNS-BSb into epoxy resin will form microcapsules with CMP1-HNS as the wall material and BDP/Sb2O5 as the core material at high temperatures, while the outer shell formed by the molecular chain of CMPs-HNS releases the nonfuel gases CO_2 and N_2, and it has been reported that BDP is an organophosphorus flame retardant and that this compound produces water, phosphoric acid, and phosphoric acid when in contact with water, metaphosphate, PO-radicals, and other reactive radicals.[64] Combustion reduces the temperature of the condensed phase and dilutes the concentration of toxic gases.[47] The phosphoric acid generated could form a glassy melt attached to the surface of the polymer microcapsule CMP1-HNS-BSb for isolation and could be used as an acid source to promote the dehydration and carbonization of the flame retardant system to prevent combustion in order to improving their thermal stability. In addition, the carbonized layer and phosphoric acid layer could also be used as a nonvolatile insulation layer to isolate heat,[65] and flame retarding mechanism of the material was basically the same as that of CMP2-HNS-BSb/EP which also had amino groups, which produced inert gases and inhibit combustion.[44] It was precisely because of the presence of flame retardant elements that when added to the epoxy resin EP and EP complex, would act as inhibitors.

5. CONCLUSIONS

In this work, we have demonstrated the synthesis of CMP hollow nanospheres (CMPs-HNS) followed by the coating of Sb_2O_5 and BDP onto the as-prepared CMPs-HNS (CMPs-HNS-BSb) by a simple immersion method to act as good flame-retardant materials and then added CMPs-HNS-BSb into the EP matrix with a certain mass ratio.

The pHRR value from MCC of CMPs-HNS-BSb was 76.5 and 73.05 W g^{-1}, respectively, which attributed to the introduction of BDP and Sb_2O_5 to act as a flame retardant. In addition, the pHRR of CMP2- HNS-BSb/EP from CC was 645.03 kW m^{-2}, which was 14.87% lower than that of pure EP at the same temperature, and the flame-retardant performance of EP was significantly improved. This is mainly because of the introduction of the flame retardant CMP2-HNS-BSb inhibiting the combustion rate and diluting the

https://doi.org/10.1021/acsomega.3c08597
ACS Omega 2024, 9, 10478−10487

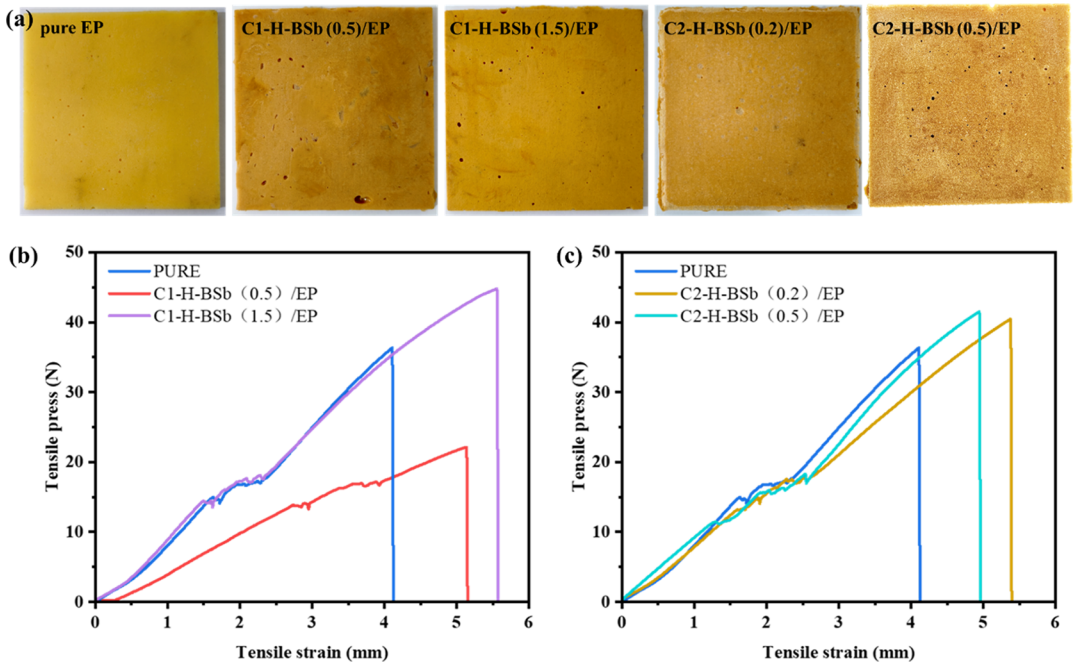

Figure 7. (a) Digital image of pure EP and CMPs-HNS-BSb/EP, (b) stress−press curves of C1-H-BSb/EP. (c) Stress−press curves of C2-H-BSb/EP.

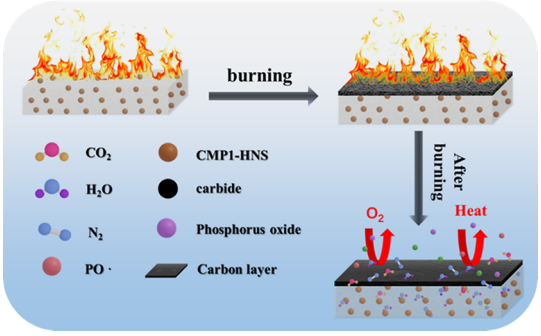

Figure 8. Flame retardant mechanism of CMP1-HNS-BSb/EP composites.

oxygen concentration to achieve the flame-retardant effect. Therefore, the CMPs-HNS-BSb may be used as a promising functional nanofillers to introduce into various flammable materials for improving their flame retardancy. More importantly, owing to the good lipophilicity and hydrophobicity of CMPs, our CMPs-HNS can also be used as a platform that can be functionalized to introduce into a variety of engineering polymeric matrix for construction of flame retardants for various applications such as aerospace, architecture, etc.

AUTHOR INFORMATION

Corresponding Authors

Chonghua Ma − *College of Petrochemical Technology, Lanzhou University of Technology, Lanzhou 730050, P. R. China*; orcid.org/0009-0009-8337-7551; Email: mch@lut.edu.cn

Zhaoqi Zhu − *College of Petrochemical Technology, Lanzhou University of Technology, Lanzhou 730050, P. R. China*; Email: zhuzhaoqi@lut.edu.cn

Author

Min Su − *College of Petrochemical Technology, Lanzhou University of Technology, Lanzhou 730050, P. R. China*

Complete contact information is available at: https://pubs.acs.org/10.1021/acsomega.3c08597

Author Contributions

C.M.: Conceptualization, methodology, writing−review and editing. M.S.: Conceptualization, methodology, resources, formal analysis. Z.Z.: Project administration, writing−review and editing.

Notes

The authors declare no competing financial interest.

ACKNOWLEDGMENTS

The authors are grateful to the National Natural Science Foundation of China (Grant No. 52163028).

REFERENCES

(1) Kim, J.; Jang, J.; Yun, S.; Kim, H. D.; Byun, Y. Y.; Park, Y. T.; Song, J. I.; Cho, C. Synergistic Flame Retardant Effects of Carbon Nanotube-Based Multilayer Nanocoatings. *Macromol. Mater. Eng.* **2021**, *306* (9), No. 2100233, DOI: 10.1002/mame.202100233.

(2) Wagner, J.; Deglmann, P.; Fuchs, S.; Ciesielski, M.; Fleckenstein, C. A.; Döring, M. A flame retardant synergism of organic disulfides and phosphorous compounds. *Polym. Degrad. Stab.* **2016**, *129*, 63−76.

(3) Mao, D.; Yang, Q.; Zhang, X.; Cheng, Y. UV-Enhanced Gas-Solid Chlorination of Polyvinyl Chloride for Cleaner Production of Chlorinated Polyvinyl Chloride. *Chem. Eng. Technol.* **2016**, *39* (5), 834−840.

(4) Martínez-Colunga, J. G.; Sanchez-Valdes, S.; Ramos-deValle, L. F.; Perez-Camacho, O.; Ramirez-Vargas, E.; Benavides-Cantú, R.; Avila-Orta, C. A.; Cruz-Delgado, V. J.; Mata-Padilla, J. M.; Lozano-Ramírez, T.; et al. Aniline-Modified Polypropylene as a Compatibilizer in Polypropylene Carbon Nanotube Composites. *Polym.-Plast. Technol. Eng.* **2018**, *57* (13), 1360−1366.

(5) Ho, B. T.; Roberts, T. K.; Lucas, S. An overview on biodegradation of polystyrene and modified polystyrene: the microbial approach. *Crit Rev. Biotechnol* **2018**, *38* (2), 308−320.
(6) Wang, H.; Wang, K.; Fan, W.; Cai, S. Rupture of swollen styrene butadiene rubber. *Polym. Test.* **2017**, *61*, 100−105.
(7) Yu, X.; Chen, X.; Zhang, J.; Gao, Y.; Liu, S. Fiber Birefringence Measurement of Single-Mode Fiber by a Polarimetric Fiber Ring Laser. *Journal of Lightwave Technology* **2018**, *36* (11), 2204−2210.
(8) Ai, L.; Yang, L.; Hu, J.; Chen, S.; Zeng, J.; Liu, P. Synergistic Flame Retardant Effect of Organic Phosphorus−Nitrogen and Inorganic Boron Flame Retardant on Polyethylene. *Polym. Eng. Sci.* **2020**, *60* (2), 414−422.
(9) Jiang, D.; Lv, S.; Cui, S.; Sun, S.; Song, X.; He, S.; Zhang, J.; An, P. Effect of thermal insulation components on physical and mechanical properties of plant fibre composite thermal insulation mortar. *Journal of Materials Research and Technology* **2020**, *9* (6), 12996−13013.
(10) Chen, C.-A.; Li, C.-C. Microencapsulating inorganic and organic flame retardants for the safety improvement of lithium-ion batteries. *Solid State Ionics* **2018**, *323*, 56−63.
(11) Luo, H.; Rao, W.; Zhao, P.; Wang, L.; Liu, Y.; Yu, C. An efficient organic/inorganic phosphorus−nitrogen−silicon flame retardant towards low-flammability epoxy resin. *Polym. Degrad. Stab.* **2020**, *178*, No. 109195.
(12) Gustavsson, J.; Wiberg, K.; Ribeli, E.; Nguyen, M. A.; Josefsson, S.; Ahrens, L. Screening of organic flame retardants in Swedish river water. *Sci. Total Environ.* **2018**, *625*, 1046−1055.
(13) Paduani, C.; Rappe, A. M. Design of New Complexes of Inorganic Salts Based on Lithium and Magnesium Hydroxides and Carbonates for Usage as Propellants and Flame Retardants. *J. Phys. Chem. A* **2016**, *120* (39), 7764−7770.
(14) Attia, N. F. Organic nanoparticles as promising flame retardant materials for thermoplastic polymers. *J. Therm. Anal. Calorim.* **2017**, *127* (3), 2273−2282.
(15) Mu, X.; Zhan, J.; Ma, C.; Pan, Y.; Chu, F.; Song, L.; Hu, Y. Integrated effect of flame retardant wrapped macromolecular covalent organic nanosheet on reduction of fire hazards of epoxy resin. *Composites Part A: Applied Science and Manufacturing* **2019**, *117*, 23−33.
(16) Calvo-Correas, T.; Ugarte, L.; Trzebiatowska, P. J.; Sanzberro, R.; Datta, J.; Corcuera, M. Á.; Eceiza, A. Thermoplastic polyurethanes with glycolysate intermediates from polyurethane waste recycling. *Polym. Degrad. Stab.* **2017**, *144*, 411−419.
(17) Gunatillake, P. A.; Dandeniyage, L. S.; Adhikari, R.; Bown, M.; Shanks, R.; Adhikari, B. Advancements in the Development of Biostable Polyurethanes. *Polym. Rev.* **2019**, *59* (3), 391−417.
(18) Kopczyńska, P.; Calvo-Correas, T.; Eceiza, A.; Datta, J. Synthesis and characterisation of polyurethane elastomers with semi-products obtained from polyurethane recycling. *Eur. Polym. J.* **2016**, *85*, 26−37.
(19) Yang, J.; Li, S.; Jiang, H.; Su, C.; Shao, Y.; Gao, Y.; Li, J. Preparation of recycled graphite/expanded polystyrene by a facile solvent dissolution method. *J. Mater. Sci.* **2019**, *54* (2), 1197−1204.
(20) Choe, J.; Kim, M.; Kim, J.; Lee, D. G. A microwave foaming method for fabricating glass fiber reinforced phenolic foam. *Composite Structures* **2016**, *152*, 239−246.
(21) Jalalian, M.; Jiang, Q.; Coulon, A.; Storb, M.; Woodward, R.; Bismarck, A. Mechanically whipped phenolic froths as versatile templates for manufacturing phenolic and carbon foams. *Mater. Des.* **2019**, *168*, No. 107658, DOI: 10.1016/j.matdes.2019.107658.
(22) Henschen, J.; Li, D.; Ek, M. Preparation of cellulose nanomaterials via cellulose oxalates. *Carbohydr. Polym.* **2019**, *213*, 208−216.
(23) Khiari, R.; Rol, F.; Brochier Salon, M.-C.; Bras, J.; Belgacem, M. N. Efficiency of Cellulose Carbonates to Produce Cellulose Nanofibers. *ACS Sustainable Chem. Eng.* **2019**, *7* (9), 8155−8167.
(24) Sun, Y.; Yan, X.; Liang, H.; Bohm, G.; Jia, L. Rubber Recycling: Mending the Interface between Ground Rubber Particles and Virgin Rubber. *ACS Appl. Mater. Interfaces* **2020**, *12* (42), 47957−47965.
(25) Lei, Y.; Tian, Z.; Sun, H.; Zhu, Z.; Liang, W.; Li, A. Self-cleaning and flexible filters based on aminopyridine conjugated microporous polymers nanotubes for bacteria sterilization and efficient PM2.5 capture. *Sci. Total Environ.* **2021**, *766*, No. 142594.
(26) Zheng, X.; Sun, R.; Qiao, L.; Guo, H.; Zheng, J.; Mai, B. Flame retardants on the surface of phones and personal computers. *Sci. Total Environ.* **2017**, *609*, 541−545.
(27) Liu, K.; Liu, C.; Hsu, P. C.; Xu, J.; Kong, B.; Wu, T.; Zhang, R.; Zhou, G.; Huang, W.; Sun, J.; et al. Core-Shell Nanofibrous Materials with High Particulate Matter Removal Efficiencies and Thermally Triggered Flame Retardant Properties. *ACS Cent Sci.* **2018**, *4* (7), 894−898.
(28) Moustakas, I. I.; Katsarou, A.; Legaki, A. I.; Pyrina, I.; Ntostoglou, K.; Papatheodoridi, A. M.; Gercken, B.; Pateras, I. S.; Gorgoulis, V. G.; Koutsilieris, M.; et al. Hepatic Senescence Accompanies the Development of NAFLD in Non-Aged Mice Independently of Obesity. *Int. J. Mol. Sci.* **2021**, *22* (7), 3446.
(29) Wang, Q.; Zhao, H.; Wang, Y.; Xie, Q.; Chen, J.; Quan, X. Determination and prediction of octanol-air partition coefficients for organophosphate flame retardants. *Ecotoxicol Environ. Saf* **2017**, *145*, 283−288.
(30) Xia, W.; Wang, S.; Wang, H.; Xu, T. Inhibitory effects of developed composite flame retardant on bituminous combustion and volatile emissions. *Journal of Cleaner Production* **2021**, *279*, No. 123538.
(31) Attia, N. F.; Elashery, S. E. A.; Zakria, A. M.; Eltaweil, A. S.; Oh, H. Recent advances in graphene sheets as new generation of flame retardant materials. *Materials Science and Engineering: B* **2021**, *274*, No. 115460.
(32) Attia, N. F. Sustainable and efficient flame retardant materials for achieving high fire safety for polystyrene composites. *J. Therm. Anal. Calorim.* **2022**, *147* (10), 5733−5742.
(33) Attia, N. F. Nanoporous carbon doped with metal oxide microsphere as renewable flame retardant for integrating high flame retardancy and antibacterial properties of thermoplastic polymer composites. *J. Therm. Anal. Calorim.* **2023**, *148* (12), 5335−5346.
(34) Liu, L.; Xu, Y.; Xu, M.; Li, Z.; Hu, Y.; Li, B. Economical and facile synthesis of a highly efficient flame retardant for simultaneous improvement of fire retardancy, smoke suppression and moisture resistance of epoxy resins. *Composites Part B: Engineering* **2019**, *167*, 422−433.
(35) Qiao, Y.; Li, Q.; Li, Q.; Yang, K.; Bai, C.; Zhang, L.; Yao, Z.; Wang, P.; Zheng, T.; Zhang, X.; et al. Improving thermal insulation properties of lightweight epoxy resin matrix composites with millimeter-sized hollow glass microspheres/epoxy hollow spheres. *Energy and Buildings* **2022**, *277*, No. 112546.
(36) Li, Q.; Razzaque, S.; Jin, S.; Tan, B. Morphology design of microporous organic polymers and their potential applications: an overview. *Science China Chemistry* **2017**, *60* (8), 1056−1066.
(37) Ahmed, D. S.; El-Hiti, G. A.; Yousif, E.; Hameed, A. S.; Abdalla, M. New Eco-Friendly Phosphorus Organic Polymers as Gas Storage Media. *Polymers (Basel)* **2017**, *9* (8), 336.
(38) Fan, Y.; Bai, W.; Mu, P.; Su, Y.; Zhu, Z.; Sun, H.; Liang, W.; Li, A. Conductively monolithic polypyrrole 3-D porous architecture with micron-sized channels as superior salt-resistant solar steam generators. *Sol. Energy Mater. Sol. Cells* **2020**, *206*, No. 110347.
(39) Zhu, Z.; Mu, P.; Fan, Y.; Bai, W.; Zhang, Z.; Sun, H.; Liang, W.; Li, A. Highly efficient solar steam generation of bilayered ultralight aerogels based on N-rich conjugated microporous polymers nanotubes. *Eur. Polym. J.* **2020**, *126*, No. 109560.
(40) Chen, T.; Sun, H.; Mu, P.; Zhu, Z.; An, J.; Liang, W.; Li, A. Fatty amines as a new family of organic phase change materials with exceptionally high energy density. *Sol. Energy Mater. Sol. Cells* **2020**, *206*, No. 110340.
(41) Ding, S. Y.; Gao, J.; Wang, Q.; Zhang, Y.; Song, W. G.; Su, C. Y.; Wang, W. Construction of covalent organic framework for

https://doi.org/10.1021/acsomega.3c08597
ACS Omega 2024, 9, 10478−10487

catalysis: Pd/COF-LZU1 in Suzuki-Miyaura coupling reaction. *J. Am. Chem. Soc.* **2011**, *133* (49), 19816−19822.
(42) Iwase, K.; Yoshioka, T.; Nakanishi, S.; Hashimoto, K.; Kamiya, K. Copper-modified covalent triazine frameworks as non-noble-metal electrocatalysts for oxygen reduction. *Angew. Chem., Int. Ed. Engl.* **2015**, *54* (38), 11068−11072.
(43) Yang, Z.; Liu, J.; Li, Y.; Zhang, G.; Xing, G.; Chen, L. Arylamine-Linked 2D Covalent Organic Frameworks for Efficient Pseudocapacitive Energy Storage. *Angew. Chem., Int. Ed. Engl.* **2021**, *60* (38), 20754−20759.
(44) Wei, H.; Wang, F.; Sun, H.; Zhu, Z.; Xiao, C.; Liang, W.; Yang, B.; Chen, L.; Li, A. Benzotriazole-based conjugated microporous polymers as efficient flame retardants with better thermal insulation properties. *Journal of Materials Chemistry A* **2018**, *6* (18), 8633−8642.
(45) Wei, H.; Wang, F.; Qian, X.; Li, S.; Hu, Z.; Sun, H.; Zhu, Z.; Liang, W.; Ma, C.; Li, A. Superhydrophobic fluorine-rich conjugated microporous polymers monolithic nanofoam with excellent heat insulation property. *Chemical Engineering Journal* **2018**, *351*, 856−866.
(46) Zhu, Z.; Wu, S.; Liu, C.; Mu, P.; Su, Y.; Sun, H.; Liang, W.; Li, A. Ionic liquid and magnesium hydrate incorporated conjugated microporous polymers nanotubes with superior flame retardancy and thermal insulation. *Polymer* **2020**, *194*, No. 122387, DOI: 10.1016/j.polymer.2020.122387.
(47) Jie, K.; Zhou, Y.; Sun, Q.; Li, B.; Zhao, R.; Jiang, D. E.; Guo, W.; Chen, H.; Yang, Z.; Huang, F.; et al. Mechanochemical synthesis of pillar[5]quinone derived multi-microporous organic polymers for radioactive organic iodide capture and storage. *Nat. Commun.* **2020**, *11* (1), 1086.
(48) Wang, Y.; Gan, Y.; Huang, J. Hyper-Cross-Linked Phenolic Hydroxyl Polymers with Hierarchical Porosity and Their Efficient Adsorption Performance. *Ind. Eng. Chem. Res.* **2020**, *59* (24), 11275−11283.
(49) Wu, S.; Zhu, Z.; Liu, C.; Su, Y.; Wang, F.; Bai, W.; Sun, H.; Liang, W.; Li, A. Facile preparation of composite flame retardantbased on conjugated microporous polymer hollow spheres. *J. Colloid Interface Sci.* **2021**, *586*, 152−162.
(50) Ma, Y.; Hu, Z.; Lu, N.; Niu, Y.; Deng, X.; Li, J.; Zhu, Z.; Sun, H.; Liang, W.; Li, A. Highly efficient solar photothermal conversion of graphene-coated conjugated microporous polymers hollow spheres. *J. Colloid Interface Sci.* **2022**, *623*, 856−869.
(51) Wang, F.; Ren, F.; Ma, D.; Mu, P.; Wei, H.; Xiao, C.; Zhu, Z.; Sun, H.; Liang, W.; Chen, J.; et al. Particle and nanofiber shaped conjugated microporous polymers bearing hydantoin-substitution with high antibacterial activity for water cleanness. *Journal of Materials Chemistry A* **2018**, *6* (1), 266−274.
(52) Zhang, L.; Pu, N.; Yu, B.; Ye, G.; Chen, J.; Xu, S.; Ma, S. Skeleton Engineering of Homocoupled Conjugated Microporous Polymers for Highly Efficient Uranium Capture via Synergistic Coordination. *ACS Appl. Mater. Interfaces* **2020**, *12* (3), 3688−3696.
(53) Du, R.; Zhang, N.; Xu, H.; Mao, N.; Duan, W.; Wang, J.; Zhao, Q.; Liu, Z.; Zhang, J. CMP aerogels: ultrahigh-surface-area carbon-based monolithic materials with superb sorption performance. *Adv. Mater.* **2014**, *26* (47), 8053−8058.
(54) Mu, P.; Sun, H.; Zhu, Z.; He, J.; Liang, W.; Li, A. Monolithic nanofoam based on conjugated microporous polymer nanotubes with ultrahigh mechanical strength and flexibility for energy storage. *Journal of Materials Chemistry A* **2018**, *6* (25), 11676−11681.
(55) Sun, H.; Zhou, P.; Ye, X.; Wang, J.; Tian, Z.; Zhu, Z.; Ma, C.; Liang, W.; Li, A. Nitrogen-doping hollow carbon nanospheres derived from conjugated microporous polymers toward oxygen reduction reaction. *J. Colloid Interface Sci.* **2022**, *617*, 11−19.
(56) Hu, Z.; Ma, Y.; Lu, N.; Yan, L.; Sun, H.; Zhu, Z.; Liang, W.; Li, A. Magnetic conjugated microporous polymer hollow spheres decorated with Fe3O4 nanoparticles for selective absorption and sterilization. *Environmental Science: Nano* **2022**, *9* (4), 1381−1390.
(57) Wang, J.; Chen, Z.; Guo, S.; Li, Y.; Lu, Z. Optimal Sprinting Pattern in Thermal Constrained CMPs. *IEEE Transactions on Emerging Topics in Computing* **2021**, *9* (1), 484−495.
(58) Lu, H.; Wilkie, C. A. Fire performance of flame retardant polypropylene and polystyrene composites screened with microscale combustion calorimetry. *Polym. Adv. Technol.* **2011**, *22* (1), 14−21.
(59) Xu, Q.; Wu, L.; Yan, X.; Zhang, S.; Dong, L.; Su, Z.; Zhong, T.; Jiang, C.; Chen, Y.; Jiang, M.; et al. Halogen-Free Flame Retardant Polypropylene Fibers with Modified Intumescent Flame Retardant: Preparation, Characterization, Properties and Mode of Action. *Polymers* **2021**, *13* (15), 2553 DOI: 10.3390/polym13152553.
(60) Spieß, B.; Metzsch-Zilligen, E.; Pfaendner, R. Mechanistic evaluation of flame retardants during UL94 standard testing via IR-camera. *Polym. Test.* **2021**, *103*, No. 107320, DOI: 10.1016/j.polymertesting.2021.107320.
(61) Pawlowski, K. H.; Schartel, B. Flame retardancy mechanisms of triphenyl phosphate, resorcinol bis(diphenyl phosphate) and bisphenol A bis(diphenyl phosphate) in polycarbonate/acrylonitrile−butadiene−styrene blends. *Polym. Int.* **2007**, *56* (11), 1404−1414.
(62) Boonkongkaew, M.; Sirisinha, K. Halloysite nanotubes loaded with liquid organophosphate for enhanced flame retardancy and mechanical properties of polyamide 6. *J. Mater. Sci.* **2018**, *53* (14), 10181−10193.
(63) Yeh, J. T.; Hsieh, S. H.; Cheng, Y. C.; Yang, M. J.; Chen, K. N. Combustion and smoke emission properties of poly(ethylene terephthalate) filled with phosphorous and metallic oxides. *Polym. Degrad. Stab.* **1998**, *61* (3), 399−407.
(64) Yang, Y.; Kong, W.; Cai, X. Two phosphorous-containing flame retardant form a novel intumescent flame-retardant system with polycarbonate. *Polym. Degrad. Stab.* **2016**, *134*, 136−143.
(65) Chen, C.; Wang, X.; Luo, T.; Zhen, H.; Yang, X.; Yang, L.; Yan, Z. Synthesis of solid reactive organophosphorus-nitrogen flame retardant and its application in epoxy resin. *J. Appl. Polym. Sci.* **2023**, *140* (33), No. e54282. (acccessed 2023/12/27)

https://doi.org/10.1021/acsomega.3c08597
ACS Omega 2024, 9, 10478−10487